Bimodal velocity distribution of atoms released from nanosecond ultraviolet laser ablation

J. Maul, S. Karpuk, and G. Huber
Institut für Physik, Johannes Gutenberg-Universität, D-55099 Mainz, Germany
(Received 9 September 2004; revised manuscript received 19 November 2004; published 27 January 2005)

We have investigated the velocity distributions of atoms released from a metallic gadolinium surface by UV laser ablation. The fluences of the nanosecond laser pulses were chosen for a pure release of neutrals and at a higher fluence level for the release of both neutrals and ions. In both cases a thermal Maxwell-Boltzmann slope has been observed for the low velocities, whereas for high velocities strong deviations from a thermal distribution have been seen. The observed velocity distribution has been explained by a bimodal structure including a thermal phase and a shockwave driven "blow-off" phase.

DOI: 10.1103/PhysRevB.71.045428 PACS number(s): 79.20.Ds, 06.30.Gv, 65.40.De

I. INTRODUCTION

The interaction of short laser pulses with a solid manifests in a variety of phenomena of higher complexity with increasing laser fluences (see, e.g., Ref. 1). Different process thresholds appear with increasing laser fluences, starting with the release of neutral particles at low fluences ($<0.5\ \mathrm{J/cm^2}$), closely followed by the threshold for ion formation. At higher fluences, Coulomb explosion is observed,[2,3] and finally a hot plasma develops.[1,3]

The response of the solid to an intense laser pulse commonly includes a local melting and vaporization of a surface spot, but also nonthermal effects like shockwave propagation[4,5] and nonthermal melting[6,7] have been demonstrated. Many investigations have been performed on metallic targets in vacuum in order to avoid additional chemical processes. The ablation process depends crucially on the laser pulse length and on its wavelength region. Ultraviolett light tends to higher ion yields, whereas infrared radiation leads to higher kinetic energies of the released ions in the plume. Moreover a higher electron temperature in the plasma phase has been reported.[8]

From the theoretical standpoint, a complete treatment of a time-limited expansion process has not yet been achieved, even not for a neutral expanding plume. Some basic insight is given by the models of Sibold and Urbassek,[9] and of Anisimov *et al.*,[10] based on fundamental principles of fluid and gas dynamics. The flow during the plume expansion is strongly governed by a single parameter, the number of monolayers removed by the laser pulse. Negligible ablation and very intense ablation fluxes can be described as a collision-free flow and by ideal gas dynamics, respectively. Here, equilibration of the flow is predicted within the formation of Knudsen layers in the vicinity of the surface.[9] The expansion is also driven by huge pressure gradients, and pressures in the range of several gigapascal can be estimated from the amount of the deposited laser pulse energy.[11]

A viable access to the dynamics of the laser ablated plume is given by the analysis of velocity distributions of released particles. For instance, it has been shown that Maxwellian and non-Maxwellian distributions, as well as different angular distributions, can be distinguished by means of resonance enhanced photoionization.[12] Commonly, the observed width of velocity distributions and especially the amount of high energy atoms are systematically underestimated by common models with a homogeneous origin (see, e.g., Ref. 13).

Within this work, we have investigated velocity distributions of neutral atoms in regimes below the plasma formation threshold during nanosecond ultraviolet laser ablation, using a pure target of metallic gadolinium. We have used a pump probe technique, mapping out different velocity classes of the released atoms by postionization at different time delays after the ablation laser pulse, and by subsequent ion detection in a time-of-flight (TOF) spectrometer. The shape of the recorded velocity distributions are discussed with regard to both thermal and nonthermal features.

II. EXPERIMENT

A Bruker Reflex III MALDI-TOF spectrometer (reflectron type TOF, flight time resolution $t/\delta t > 250$ in the linear detection mode, $t/\delta t > 1100$ in the reflection mode for the mass range of gadolinium ions) has been combined with a pulsed frequency tripled Nd: yttritium-aluminum-garnet (YAG) laser (Quantel Brilliant, $\lambda = 355$ nm, pulse length $\tau \sim 4$ ns) for posterior ionization of laser ablated neutral atoms. Thereby the residual gas pressure in the vacuum apparatus is kept at $p \sim 10^{-7}$ mbar. A brief schematic representation of the ion source setup is shown in Fig. 1, and further experimental details about the complete setup are given in Ref. 14.

Here, a high purity gadolinium metal foil (Goodfellow) was mounted on the target holder, and its surface was cleaned by ~1000 pulses of the MALDI-TOF nitrogen desorption laser (Laser Science Inc., VSL-337 ND, $\lambda = 337$ nm, $\tau \sim 4$ ns) at a fluence of $\sim 0.25\ \mathrm{J/cm^2}$. The release of neutral atoms and ions ablated by pulses of the focused nitrogen laser pulses (ablation spot diameter $\sim 20\ \mu$m) has been observed via the TOF spectrometer. During the free ballistic expansion the neutrals have been postionized by the light of the frequency tripled Nd:YAG laser and have been subsequently extracted into the TOF spectrometer (linear detection mode with continuous ion extraction). Its pulses propagated parallel to the target surface at a fixed distance of $d \sim 0.65$ mm with a flat elliptical focus ($5 \times 0.5\ \mathrm{mm^2}$). The Nd:YAG beam geometry was additionally controlled via a

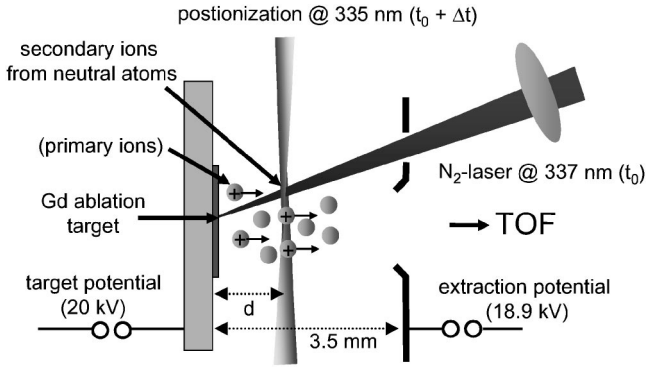

FIG. 1. Schematic view of the ion source setup in the combined laser system. A nitrogen ablation laser is used for material release from a gadolinium metal target, and the third harmonic of a Nd:YAG laser is used for probing the released neutral atoms. Both primary ions from ablation and postionized neutrals are subsequently detected by means of a TOF spectrometer.

charge coupled device (CCD) camera at the focus of a weak split beam before entering the ion source.[14]

The delay between laser ablation and postionization was controlled by a digital delay generator (Stanford Research DG 535) in steps of 100 ns. This time structure appears in the TOF spectrum since the ions were extracted continuously by an electrical field of 310 V/mm between the target and the extraction electrode, as it is apparent from Fig. 1. Thus the ions from postionized neutrals were delayed relative to the ablation ions. With the known delay Δt and traveling distance d between target and laser beam, the velocity classes $v := d/\Delta t$ are determined and their yield is given by the TOF spectrum.

III. THRESHOLD FLUENCES

At first, threshold fluences of the charge states present in the laser ablated plume were analyzed. At a fixed time delay of $\Delta t = 600$ ns both relative yields of ablated ions and of postionized atoms were recorded at different ablation laser fluences, and identified from the TOF spectra, as shown in Fig. 2.

At the ablation onset (~ 0.15 J/cm^2), only neutral particles are released. At a slightly higher laser fluence (~ 0.2 J/cm^2), the ion formation threshold is trespassed. Both yields of singly charged gadolinium and of postionized neutral gadolinium rise rapidly after their formation thresholds. With increasing laser fluences (>0.25 J/cm^2), also doubly charged gadolinium ions are found. Remarkably, the signal for doubly charged Gd ions decreases (>0.35 J/cm^2) and nearly vanishes (>0.5 J/cm^2) for higher fluences, even though more laser energy is applied to the target spot. The emitted electrons are usually at least one order of magnitude faster than the ablation ions (see Ref. 15), so that recombination between ions and electrons can be excluded. Since the plume density increases continuously with the laser fluence, charge exchange between neutrals and doubly charged ions can take place. The decrease of the doubly charged ion signal can therefore be interpreted by charge

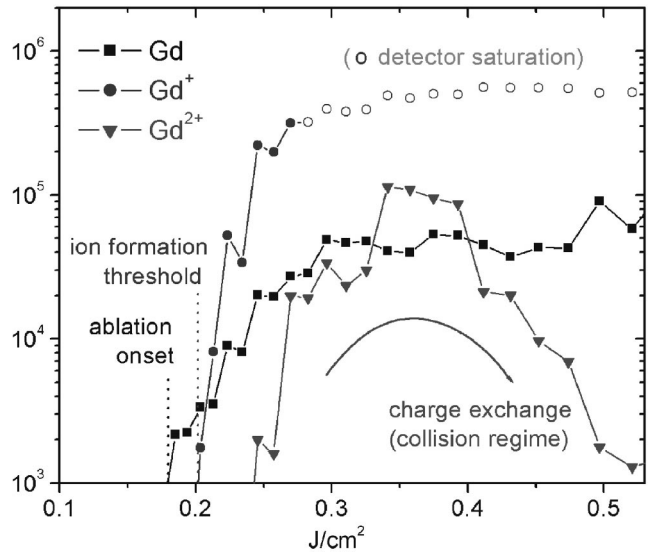

FIG. 2. Charge states present in the laser ablated plume.j Postionized neutral gadolinium atoms, as well as singly and doubly charged gadolinium ions are extracted from the TOF spectra for different ablation laser fluences. Thresholds for ablation and for ion formation are marked, as well as a regime for collisional charge exchange.

transfer between neutral atoms and doubly charged ions during collisions in gas phase, corresponding to a regime of ideal gas dynamics as described in Ref. 9.

With respect to further investigations in Sec. IV, it should be anticipated that collisional conditions might change from the direct vicinity of the surface, where, e.g., the formation of Knudsen layers can occur, to a more remote region of free expansion.

IV. VELOCITY CLASS DISTRIBUTIONS AND DISCUSSION

For basic insight into the plume kinematics, the regime directly above the ablation onset can be considered to be especially valuable for several reasons: This regime is strongly dominated by the processes in the surface ablation spot, and not by interactions between particles in gas phase, e.g., by Coulomb repulsion and atomic collisions. It can be expected that the ablation process appears in its most fundamental form, including a ballistic expansion of neutral atoms from the irradiated spot.

In the following, we discuss velocity class distributions of laser ablated neutral gadolinium atoms obtained from a pump-probe experiment: The ablation laser pulse thereby realizes the "pump process," and the "probe process" is performed by the frequency-tripled Nd:YAG laser beam. From the series of time-of-flight spectra of nonresonantly postionized gadolinium, peak heights of the $^{160}Gd^+$ ion signal have been extracted from each spectrum representatively, in order to obtain a time-of-flight distribution of gadolinium atoms in the plume. For each TOF spectrum, 600 pump-probe sequences were summed up, and for each delay two sum spectra have been recorded. The time-of-flight distributions were

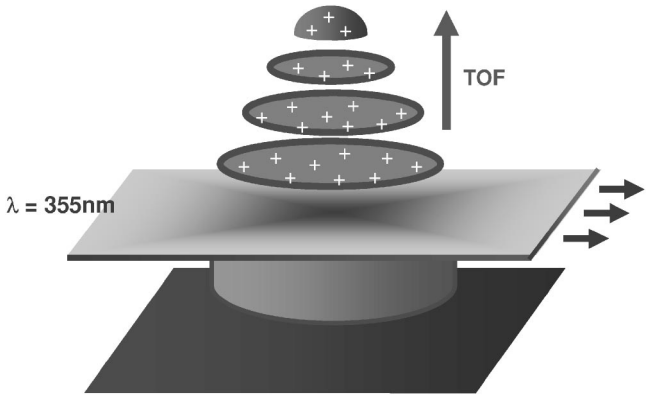

FIG. 3. Schematic representation of the pump probe process, as inferred from Fig. 1. Laser ablation from the gadolinium target shown at the bottom (pump pulse from nitrogen laser, $\lambda = 337$ nm, $\tau \sim 4$ ns) produces an expanding atom plume. At a distance of ~ 0.65 mm and after different time delays Δt, postionization (probe pulse, $\lambda = 335$ nm, $\tau \sim 4$ ns), different velocity classes of neutral atoms are mapped out and detected by means of a TOF spectrometer.

then converted into distributions of velocity classes, defined by the probe pulse geometry relative to the gadolinium ablation target, as illustrated in Fig. 3.

Figure 4 shows a velocity class distribution in the low laser fluence regime directly above the ablation onset (~ 0.18 J/cm^2), where no ions are produced. In Fig. 5, a velocity class distribution recorded in the higher regime directly above the ion formation threshold at a fluence of ~ 0.22 J/cm^2 is shown. In that case, only the high velocity wing could not be recorded, because of interferences in the TOF signal from primary ablation ions.

For the evaluation of the velocity class distributions, we have used a modified Maxwell-Boltzmann fitting function $f(v,T)$ in order to describe the expansion of a thermal vapor from a melted target spot

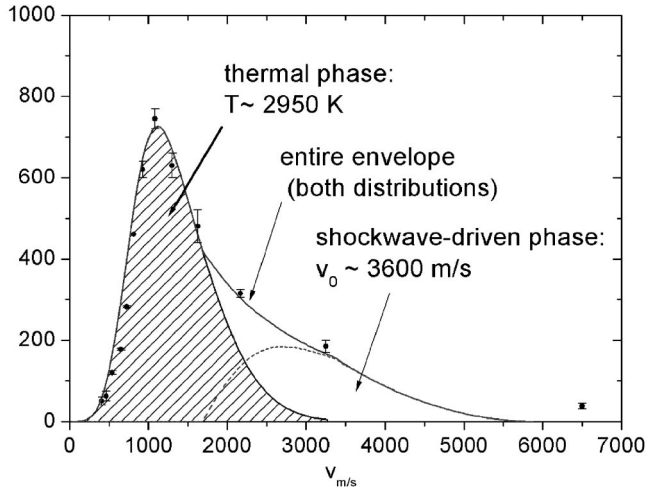

FIG. 4. Velocity class distribution obtained in the low fluence regime (~ 0.18 J/cm^2). A thermal contribution is fitted by a Maxwell-Boltzmann distribution, whereas a nonthermal phase is modeled for higher velocity classes. The entire envelope contains both contributions.

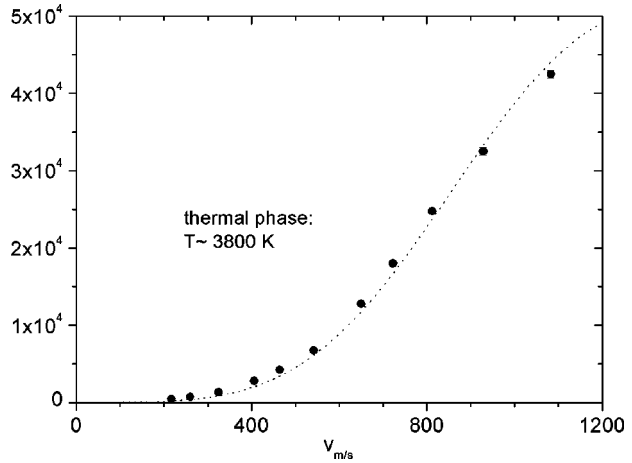

FIG. 5. Slope of the velocity class distribution from the regime above the ion formation threshold (~ 0.22 J/cm^2). A Maxwell-Boltzmann distribution $\tilde{f}$ is used for fitting the data.

$$f(v,T) \propto v^3 \exp\left[-\frac{m(v-v_{CMS})^2}{2kT}\right].$$

Here, the center-of-mass velocity v_{CMS} accounts for the limited plume expansion into the hemisphere above the target plane. It is identified by the average velocity of the atoms in the expanding gas, as given by[16]

$$v_{CMS} = \frac{3\sqrt{\pi}}{4}\sqrt{2kT/m}.$$

Within this frame, the measured velocity class distributions are compared to a model with a single intrinsic parameter T.

To be more precise, the Maxwell-Boltzmann distribution for the expanding gas has still to be adapted to the probe geometry, where the probe laser selects velocity classes in a volume V of definite thickness Δd around a central position d parallel to the target plane. Using an adjustable slit, the $1/e$-waist of the focused frequency-tripled Nd:YAG beam is determined to 300 μm, and 90% of the laser pulse energy is found to be localized in a domain of 500 μm around the central beam position $d = 650$ μm.

The adaptation of the Maxwell-Boltzmann distribution to the probe laser geometry has been realized by a transformation

$$\tilde{f}(v,T) \sim \int_V f[v\ \cos(\Theta)\cdot z/d, T]dV(\Theta,z),$$

where the numerical integration of the distribution $f(v,T)$ over the ionization volume V is performed by introducing two auxiliary spatial variables Θ and z, the acceptance angle Θ of the spectrometer at the postionization location, which is in good approximation given by $\pi/6 \geqslant \Theta \geqslant 0$, and the extension z of the probe laser beam parallel to the target plane [we choose $z \sim (650 \pm 250)$ μm].

In order to extract the temperature from velocity class distributions, the modified Maxwell-Boltzmann fits $\tilde{f}$ have been applied to the data shown in Figs. 4 and 5. Apparently,

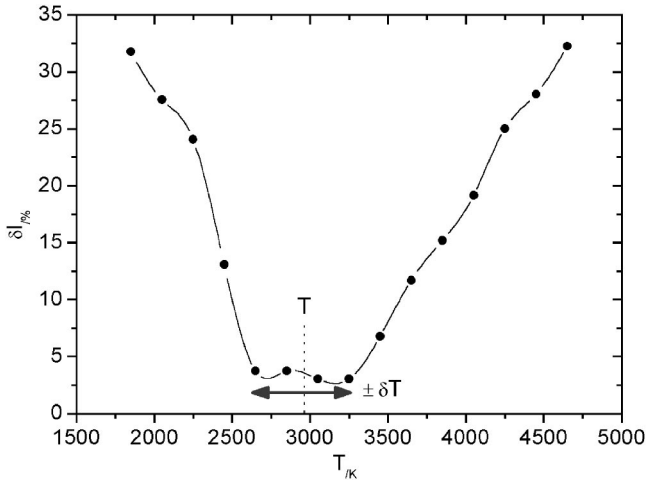

FIG. 6. Relative deviation δI of the Maxwell-Boltzmann distribution $\tilde{f}$ from the velocity distribution in Fig. 3 as a function of the temperature. The temperature T and the corresponding error δT are obtained from the extended minimum of the deviation δI.

there is a strong asymmetric broadening in Fig. 4, which is not in agreement with a pure thermal distribution. The nonthermal contribution will be explained later.

In Fig. 4, the modified Maxwell-Boltzmann fit has been applied to the first ten data points, belonging to the lower velocity classes. Here, a good agreement with a thermal distribution has been found. The modified Maxwell-Boltzmann distribution fitting these data has been probed with different temperatures as seen in Fig. 6. The relative error δI remains below 5% at $T \pm \delta T \sim (2950 \pm 300)$ K and increases rapidly outside. This procedure determines the temperature error. In the same way, a modified Maxwell-Boltzmann fitting curve $\tilde{f}$ has been applied to the measured low velocity wing in Fig. 5 obtained at a higher ablation laser fluence. A temperature of $T \sim 3800$ K is extracted, which is significantly higher compared to the lower laser fluence regime of Fig. 3. Thereby, the low velocity wing is again attributed to a purely thermal distribution, as it is justified by the good agreement of the one-parameter fitting curve with the data.

For higher velocity classes in Fig. 4, $v \geqslant 1800$ m/s, a significant broadening of the measured velocity class distribution is visible, resulting in a strong deviation from a thermal distribution. In Refs. 12 and 17, a similar behavior has been observed, and in Ref. 12 a nonthermal origin has been already suggested. In the following, we use a simple kinematical model, where the release of the fastest particles is inferred from a shockwave, induced by the high momentum transfer from the ablation by the short laser pulse. For this, layers immediately behind the upper surface layer should be considered in particular. Typically, the absorption of laser light in a metal takes place within a penetration depth of $\sim \lambda/10$, when the laser frequency is above the Langmuir frequency of the metal. In the case of UV light, the penetration usually can be expected to be even higher, especially near the plasma frequency. This can result in subsurface heating, from which an internal pressure affects the upper surface layer, thus enabling a fast release of atoms.

Due to a small lateral extension of the ablation spot of about 20 μm in diameter within our experiment, the ablation zone can be regarded in good approximation as a pointlike source for particle release. In our model, we therefore have assumed a completely hemispherical expansion of a thin shockwave-driven material front away from the target surface, as it is furthermore supported by photographic sequences of expanding plumes from nanosecond UV laser ablation under similar experimental conditions, shown, e.g., in Ref. 18.

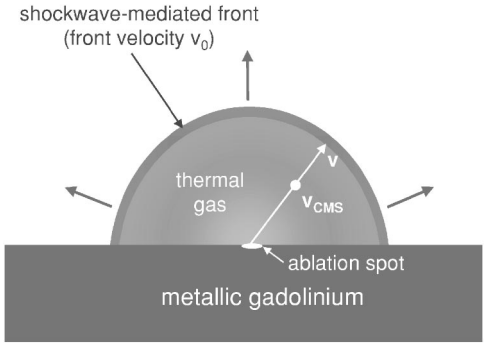

FIG. 7. Schematic illustration of the plume expansion, as inferred from the models for a combined thermal and a shockwave-driven particle release. Thereby a shockwave-driven hemisphere with front velocity v_0 precedes the expansion of a thermal gas with center-of-mass velocity v_{CMS}.

It should be mentioned that the formation of shockwaves after pulsed laser irradiation is per se a well-known phenomenon (see, e.g., in Refs. 4 and 5). Laser shock techniques are systematically used in material science, e.g., for investigating debonding of surface coatings from substrates.[19,20] The fast material release, originating from mechanical stress, can be understood by the Navier-Stokes equation from fluid dynamics

$$\rho \frac{\partial u}{\partial t} = - \nabla p,$$

where u is the flow velocity at the vacuum boundary, ρ is the mass density in the condensed ablation zone, and ∇p is the pressure gradient across the boundary. The mass density in the high vacuum region at $p \sim 10^{-7}$ mbar is thereby neglected. Because of the negative pressure gradient ∇p across the vacuum boundary, the flow velocity u is increased compared to the sound speed c_0, which characterizes the shockwave propagation in the solid metal. A similar consideration has also been presented, e.g., in Ref. 5. For solid gadolinium, the speed of sound is $c_0 = \sqrt{\varepsilon/\rho} \approx 2190$ m/s, where $\rho = 7.9$ g/cm^3 is the mass density of solid gadolinium, and $\varepsilon = 37.9$ GPa is the corresponding elastic modulus.

By projecting the hemispherical expansion of a shockwave-driven material front with negligible thickness (see Fig. 7 for illustration) onto the probe laser geometry, a shockwave-related contribution is attributed to the wing of high velocity classes in Fig. 4. Here, a material front velocity $v_0 \sim 3600$ m/s is extracted within this one-parameter model, indicating a supersonic expansion into vacuum when compared to the speed of sound in the solid, $v_0 > c_0$.

The combination of both the thermal and the shockwave-driven contribution is marked in Fig. 4 by the indication of the entire envelope; the complete scenario is also illustrated schematically in Fig. 7. The entire distribution agrees reasonably with the measured velocity class distribution. Some small errors might occur from the deviation of the plume shape from a completely hemispherical geometry. Usually, the plume geometry is expressed in terms of $\cos^n(\Theta)$, where Θ is the polar angle relative to the surface normal.[12] For $n<1$, the plume shape is oblate, and for $n>1$, the geometry is prolongated in flight direction.

It should be mentioned that similarly shaped velocity distributions have been observed in other experiments (e.g., in Ref. 13), where the high velocity part could not be interpreted in a natural way. From our interpretation of a bimodal distribution, both the commonly accepted assumption of a thermal contribution during nanosecond laser ablation, and the frequently observed deviation to higher velocities, are brought into accord. Recent investigations performed with fast flash imaging of nanosecond matrix assisted laser desorption/ionization (MALDI) plumes[21] support our interpretation of a heterogeneous ablation structure for short (nanosecond) laser pulses, whereas longer laser pulses ($\sim$100 ns) were found to introduce a more homogeneous ablation in that work. A bimodal structure was also found in the time-of-flight transient from ultrashort femtosecond laser ablation of metallic silicon.[22]

V. CONCLUSIONS

From a velocity-selective pump-probe experiment of laser ablated neutral atoms, both thermal and nonthermal features of the expanding plume have been discussed. Whereas low velocity classes show a good agreement with a thermal distribution of released atoms, a significant deviation from a Maxwell-Boltzmann distribution has been observed for the highest velocity classes. This behavior can be attributed to a shockwave-driven phase, with a material front velocity exceeding the sound speed in the solid target. The presented results might be helpful for the interpretation of further velocity selective laser ablation experiments.

[1] R. E. Russo, X. Mao, and S. S. Mao, Anal. Chem. **74**, 71A (2002).

[2] R. Stoian, A. Rosenfeld, D. Ashkenasi, I. V. Hertel, N. M. Bulgakova, and E. E. B. Campbell, Phys. Rev. Lett. **88**, 097603 (2002).

[3] R. Stoian, D. Ashkenasi, A. Rosenfeld, and E. E. B. Campbell, Phys. Rev. B **62**, 13 167 (2000).

[4] A. H. Shen, T. J. Ahrens, and J. D. O'Keefe, J. Appl. Phys. **93**, 5167 (2003).

[5] J. Lee and M. F. Becker, J. Appl. Phys. **89**, 8146 (2001).

[6] C. W. Siders *et al.*, Science **286**, 1340 (1999).

[7] A. Rousse *et al.*, Nature (London) **410**, 65 (2001).

[8] L. Torrisi, S. Gammino, L. Ando, V. Nassisi, D. Doria, and A. Pedone, Appl. Surf. Sci. **210**, 262 (2003).

[9] D. Sibold and H. M. Urbassek, Phys. Rev. A **43**, 6722 (1991).

[10] S. I. Anisimov, D. Bäuerle, and B. S. Luk'yanchuk, Phys. Rev. B **48**, 12 076 (1993).

[11] K. Sokolowski-Tinten, J. Bialkowski, A. Cavalleri, D. von der Linde, A. Oparin. J. Meyer-ter-Vehn, and S. I. Anisimov, Phys. Rev. Lett. **81**, 224 (1998).

[12] V. G. Bordo and H. G. Rubahn, Chem. Phys. Lett. **309**, 143 (1999).

[13] A. V. Gusarov and I. Smurnov, J. Phys. D **34**, 1147 (2001).

[14] J. Maul *et al.*, Nucl. Instrum. Methods Phys. Res. B **226**, 644 (2004).

[15] B. Toftmann, J. Schou, T. N. Hansen, and J. G. Lunney, Phys. Rev. Lett. **84**, 3998 (2000).

[16] N. F. Ramsey, in *Molecular Beams*, edited by N. F. Mott and E. C. Bullard, The International Series of Monographs on Physics (Oxford University Press, New York, 1956).

[17] H. Nishikawa, M. Kanai, T. Kawai, and S. Kawai, J. Appl. Phys. **33**, L1090 (1994).

[18] R. Srinivasan, B. Braren, K. G. Casey, and M. Yeh, Lambda Highlights **21**, 1 (1990).

[19] M. Boustie, E. Auroux, J.-P. Romain, A. Bertoli, and D. Manesse, Eur. Phys. J. A **5**, 149 (1998).

[20] M. Boustie, E. Auroux, J.-P. Romain, and M. Jeandin, J. Phys.: Condens. Matter **14**, 10839 (2002).

[21] A. Rohlfing, C. Menzel, L. M. Kukreja, F. Hillenkamp, and K. Dreisewerd, J. Phys. Chem. B **107**, 12275 (2003).

[22] W. G. Roeterdink, L. B. F. Juurlink, O. P. H. Vaughan, J. Dura Diez, M. Bonn, and A. W. Kleyn, Appl. Phys. Lett. **82**, 4190 (2003).